Supplemental materials

Farnesoid X receptor and G protein-coupled bile acid receptor 1 double knockout mice: a potential mouse model for liver fibrosis

Jessica M. Ferrell, Preeti Pathak, Shannon Boehme, Tricia Gilliland, and John Y.L. Chiang

Supplemental methods:

Dietary Treatments

Cholic acid: Male C57BL/6J wild type, *Fxr*$^{-/-}$, *Tgr5*$^{-/-}$ and *Fxr*$^{-/-}$/*Tgr5*$^{-/-}$ mice were given *ad libitum* access to chow diet supplemented with cholic acid (0.5% w/w, Sigma-Aldrich, St. Louis, MO) for 2 weeks. **Cholestyramine:** Male C57BL/6J wild type and *Fxr*$^{-/-}$/*Tgr5*$^{-/-}$ were given *ad libitum* access to chow diet supplemental with the bile acid binding resin cholestyramine (2% w/w; Sigma-Aldrich) for 2 weeks. **Western diet:** Male C57BL/6J wild type, *Fxr*$^{-/-}$, *Tgr5*$^{-/-}$ and *Fxr*$^{-/-}$/*Tgr5*$^{-/-}$ mice were given *ad libitum* access to Western diet (42% kcal from fat, 0.2% cholesterol, Harlan Teklad TD.88137) for 16 weeks. After dietary treatment, mice were sacrificed during the fed state, except where noted, from approximately 9-11 am and tissues were collected for analysis.

Glucose and insulin tolerance tests: Glucose tolerance testing was in 4 month-old male wild type, *Fxr*$^{-/-}$, *Tgr5*$^{-/-}$ and DKO mice maintained on chow or Western diet. Mice were IP injected with D-glucose dosed at 2 g/kg body weight following a 16 hr fast. Insulin tolerance was tested by IP injection of insulin (Humulin R; Eli Lilly, Indianapolis, IN) dosed at 0.75 U/kg body weight following a 5 hr fast. Blood samples were collected via tail vein and blood glucose was measured using a OneTouch Ultra Mini glucometer (LifeScan; Milpitas, CA).

Metabolic analysis: Metabolic analysis of 4-5 month old male wild type and DKO mice fed chow or Western diet was performed using a Comprehensive Lab Animal Monitoring System (CLAMS) (Columbus Instruments; Columbus, OH). The CLAMS utilizes indirect calorimetry to determine metabolic performance continuously. Briefly, mice were housed individually in sealed clear Plexiglass cages through which fresh room air was continuously passed at 0.5 L/min. Via O_2 and CO_2 sensors, exhaust air was sampled in each cage in succession at 2 min intervals over 24 hr. O_2 consumption (V_{O2}), CO_2 production (V_{CO2}), respiratory exchange ratio (RER [V_{CO2}/V_{O2}], an estimate of fuel usage) and energy (heat) production were calculated and recorded electronically over 24 hr for each mouse (following a 48 hr acclimation period). Total locomotor activity (measured by *x*, *y* and *z* axis infrared beam breaks) and diet consumption were also recorded electronically for each mouse. Weekly body weight was recorded in all mice. An EchoMRI 3-in-1 Body Composition Analyzer (EchoMRI; Houston TX) was used to record measurements of fat and lean tissue mass in live mice before metabolic analysis. After completion of recording, mice were sacrificed and tissues were then collected for analysis.

Serum and tissue analyses: Tissue lipids were extracted by homogenizing 100 mg frozen liver in 500 µL PBS, then 700 µL of a chloroform: isopropanol: NP-40 (7:11:0.1 v/v) solution was added and the samples were vortexed and incubated in a sonicating water bath for 1 hr. Samples were centrifuged at 13,000 rpm for 10 min and the organic layer was collected and dried at 55°C. The lipids were re-suspended in 200 µL cholesterol assay buffer (BioVision Inc., Milpitas, CA). Lipid content was assayed using cholesterol and triglyceride reagents (Infinity, Thermo Scientific) and a NEFA kit (Wako Diagnostic, Richmond, VA). Homogenized liver was assayed for y-glutamyltransferase (Thermo Scientific), thiobarbituric acid reactive substances (TBARS; Cayman Chemical, Ann Arbor, MI), superoxide dismutase (SOD; Cayman Chemical), and hydroxyproline (BioVision Inc.), and homogenized liver and serum were assayed for

alkaline phosphatase (BioVision Inc.). Serum was analyzed for ALT (Abcam, #ab105134) and AST (#ab105135).

Histology: Tissues were fixed in 10% buffered formalin and were processed overnight for paraffin embedding. Paraffin sections (10 μM) were stained with hematoxylin and eosin (H&E), Picro-Sirus Red, Mason's Trichrome, and α-smooth muscle actin (α-SMA). Separate tissue samples were embedded in OCT and were cryosectioned at 10 μM for Oil Red O staining. Images were visualized using an Olympus BX40F microscope and captured by Olympus LCMicro software.

Bile acid analysis

Bile acid pool size: Bile acids were extracted from 100 mg frozen liver and whole intestine by a series of ethanol extractions (95%, followed by 85%) and a chloroform: methanol extraction (2:1 v/v), each overnight in a 60°C water bath. Gallbladder bile was dissolved in 85% ethanol. Bile acid content in tissue and serum was quantified using a Total Bile Acid Assay kit (Catalog #DZ042A-K; Diazyme Laboratories, Poway, CA). Liver bile acid content was determined by back-calculation using whole liver weight. Bile acid pool size was determined by totaling bile acid content in whole liver, gallbladder and intestine.

Bile acid composition: Bile acid composition in gallbladder bile of fasted wild type and DKO mice were analyzed as described previously by UHPLC-QTOFMS (1).

Quantitative real time PCR analysis of mRNA: Total RNA was isolated from frozen tissue using Trizol (Sigma-Aldrich), followed by chloroform extraction and isopropanol precipitation. Reverse transcription was performed using RETROscript Reverse Transcription Kits (Catalog #AM1710) and 2 μg hepatic or intestinal RNA. Real-time PCR was performed for quantitative mRNA assay using Taqman primer/probe sets (Applied Biosystems, Foster City, CA), except for

S1pr2 (BioRad, Hercules, CA). Relative mRNA expression was quantified using the ΔΔCt method and *Gapdh* was used as an internal standard.

Next Generation RNA-Sequencing

Transcriptome profiling with RNA-Sequencing (RNA-Seq) was performed using a directional mRNA-Seq strategy (2, 3). Briefly, indexed sequencing libraries were prepared from total RNA (100 ng) preparations using the NEBNext Ultra Directional RNA Library Prep Kit (New England BioLabs, Ipswich, MA), according to the manufacturer's protocol for poly (A) RNA capture, cDNA synthesis, blunt-ending and 3′-A tailing, ligation of indexed adapters, and high-fidelity PCR enrichment of the libraries; strand marking" is accomplished by incorporation of dUTP in place of dTTP during second strand cDNA synthesis (2, 3). Libraries were then combined and multiplexed sequenced (2x150 bp, paired-end, <10 samples/lane) on an Illumina HiSeq 4000 sequencing system in order to achieve >30 million reads per sample, which is ample for general gene expression profiling. De-multiplexed raw sequence data (FASTQ) was analyzed with a HISAT-StringTie-Ballgown pipeline (4) for read mapping to the current reference mouse genome assembly (GRCm38/mm10) (5), followed by transcript assembly and quantification of expression values as FPKM (fragments per kilobase of exon per million mapped sequence reads) (6). Gene- and transcript-level FPKM expression values were then passed onto Ballgown (7) for identification of differentially expressed genes (DEGs; $p<0.05$, FDR<0.05) in *Fxr*$^{-/-}$, *Tgr5*$^{-/-}$, and *Fxr*$^{-/-}$ and *Tgr5*$^{-/-}$ double knockout (DKO) mice. The molecular relatedness of these models, and co-expressed gene modules defining these, were then delineated and visualized by principal component analysis (PCA) and hierarchical clustering. Functional enrichment analysis using g: Profiler (8) and Gene Set Enrichment Analysis (GSEA) (9) were applied in order to gain insight into the biological and mechanistic implications of the DEGs that are in common, or unique, to the different KO gene mouse models. Together, these system biology approaches identified statistical enrichment, or over-representation, of genes for

Gene Ontology (GO) annotations (10) (biological processes, molecular function), regulatory motifs, signal transduction pathways, and overlap with annotated gene sets from the Molecular Signature Database (MSigDB v6.1, release October 2017), which include collections specific for different biological states and metabolic signatures.

Immunoblot analyses: Total proteins were extracted from individual mouse liver tissue samples, and protein lysates were dissolved in modified RIPA buffer for immunoblot analysis. Protein concentration was determined by Pierce BCA analysis (ThermoFisher Scientific, Inc.) and 40 µg total protein was loaded in each well (n=3). Samples were separated by SDS-PAGE gel electrophoresis (BioRad) and trans-blotted onto PVDF membrane. Blots were blocked for 1 hr in 5% non-fat dry milk in TBST followed by overnight incubation at 4°C with antibodies against phospho-AKT (#4060S, Cell Signaling Technology, Danvers, MA), total AKT (#9272S, Cell Signaling Technology), Cyp8b1 (ab191910, Abcam), Cyp7b1 (ab138497, Abcam), and Cyp27a1 (ab126785, Abcam), and Gapdh (#5174; Cell Signaling Technology) was used as an internal control. Microsomal protein was isolated from 25 mg frozen liver tissue with a chilled Dounce homogenizer and RIPA buffer. Samples were ultracentrifuged at 35,000 rpm for 1 hr and the pellet was resuspended in RIPA buffer. Microsomal protein was probed for Cyp7a1 (#ab65596, Abcam) and Calnexin (ab22595, Abcam) was used as an internal control. After overnight incubation, blots were washed 3x in TBST for 10 min each, and were then incubated with goat anti-rabbit secondary antibody (#ab6721, Abcam) at room temperature for 90 min. Blots were visualized by an image scanner (ImageQuant LAS 4000, GE Healthcare Bio-Sciences; Pittsburgh, PA) and were quantified using ImageJ software (NIH, Bethesda, MD).

Cyp7a1 activity assay: Mouse liver microsomes were isolated for the analysis of Cyp7a1 enzyme activity using HPLC-based methods as described previously (11).

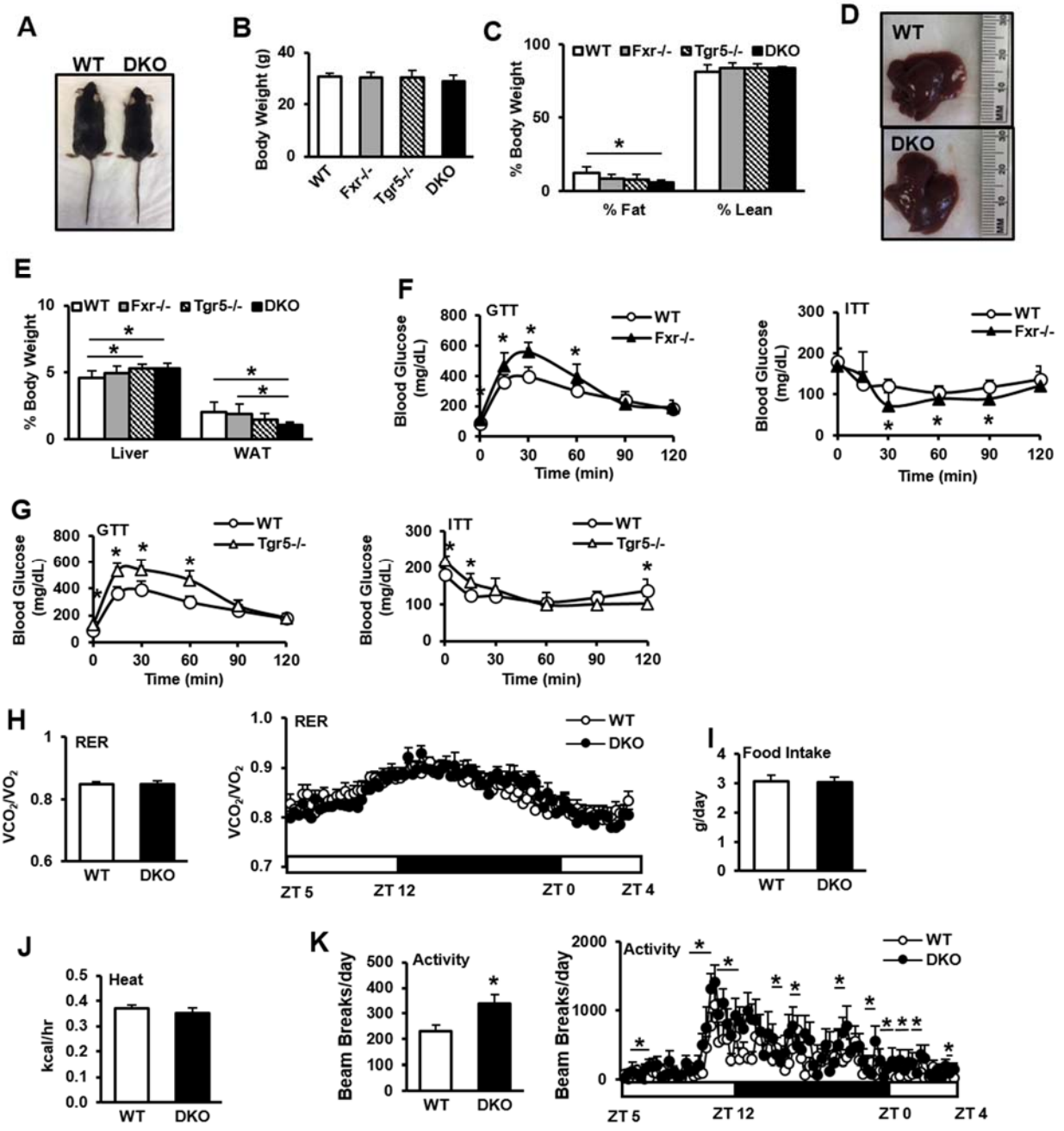

Supplemental Figure 1. Male wild type, *Fxr*$^{-/-}$, *Tgr5*$^{-/-}$, and *Fxr*$^{-/-}$/*Tgr5*$^{-/-}$ (DKO) mice, n=6-9. **A.** Male wild type mouse (left) and DKO mouse (right). **B.** Male wild type, *Fxr*$^{-/-}$, *Tgr5*$^{-/-}$, and DKO adult body weight. **C.** Body composition. **D.** Male wild type mouse liver (top) and DKO mouse liver (bottom). **E.** Liver and white adipose tissue (WAT) weight normalized to body weight. **F.**

Male wild type and *Fxr*$^{-/-}$ glucose tolerance test (left) and insulin tolerance test (right). G. Male wild type and *Tgr5*$^{-/-}$ glucose tolerance test (left) and insulin tolerance test (right). **H.** Respiratory exchange ratio (left) and over 24 hr (right). **I.** Average daily food intake. **J.** Average heat production. **K.** Average daily locomotor activity (left) and over 24 hr (right). WT, wild type mice; Fxr-/-, Fxr single knockout mice; Tgr5-/-, Tgr5 single knockout mice, DKO, *Fxr*$^{-/-}$/*Tgr5*$^{-/-}$ double knockout mice; ***** indicates $p<0.05$.

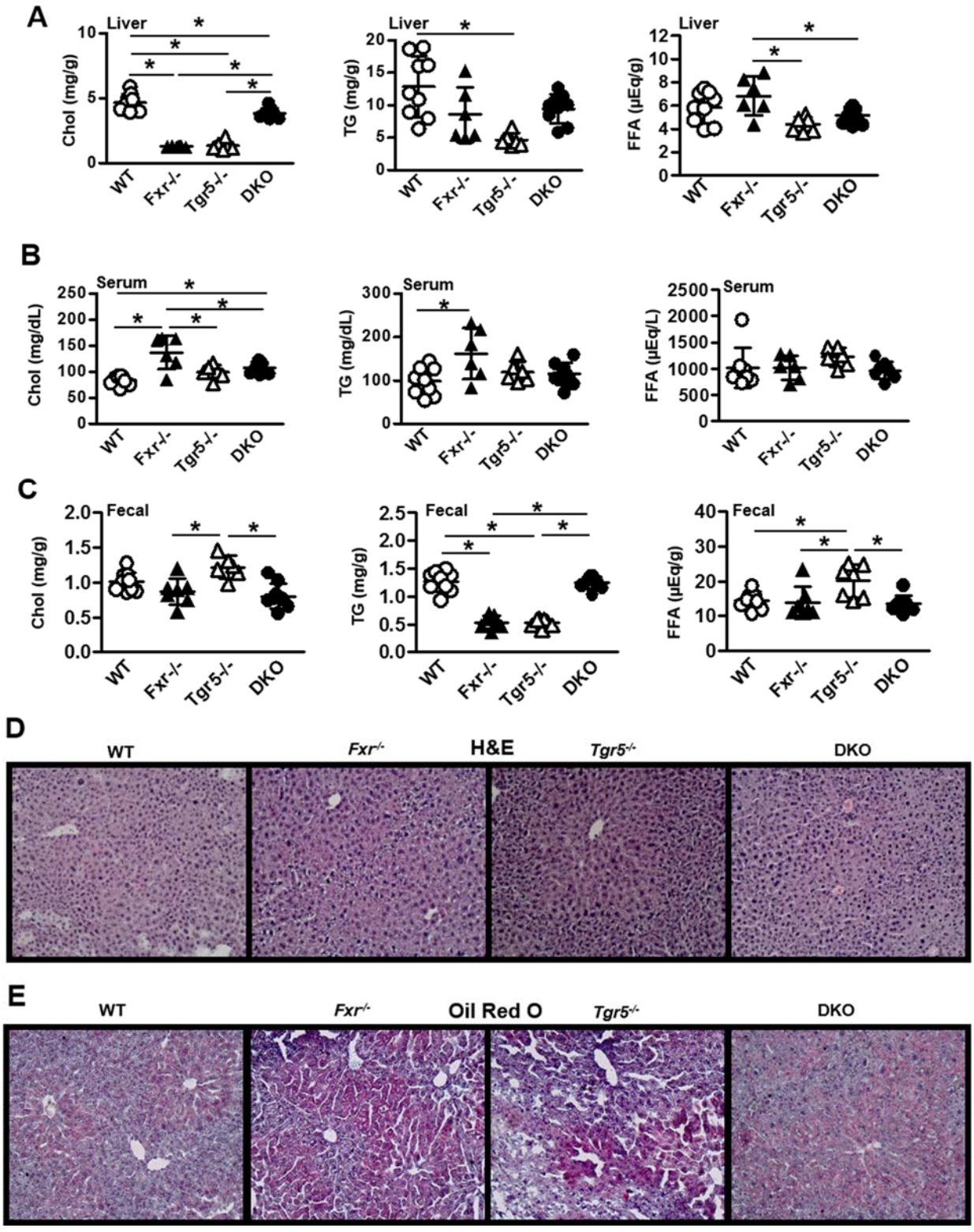

Supplemental Figure 2. Male wild type, *Fxr*$^{-/-}$, *Tgr5*$^{-/-}$, and *Fxr*$^{-/-}$/*Tgr5*$^{-/-}$ (DKO) mice, n=6-9. **A.** Liver cholesterol (left), triglycerides (middle) and free fatty acids (right). **B.** Serum cholesterol

(left), triglycerides (middle) and free fatty acids (right). **C.** Fecal cholesterol (left), triglycerides (middle) and free fatty acids (right). **D.** Representative image of liver hematoxylin & eosin staining (10x). **E.** Representative image of liver Oil Red O staining (10x). WT, wild type mice; Fxr-/-, Fxr single knockout mice; Tgr5-/-, Tgr5 single knockout mice, DKO, *Fxr*$^{-/-}$/*Tgr5*$^{-/-}$ double knockout mice; * indicates $p<0.05$.

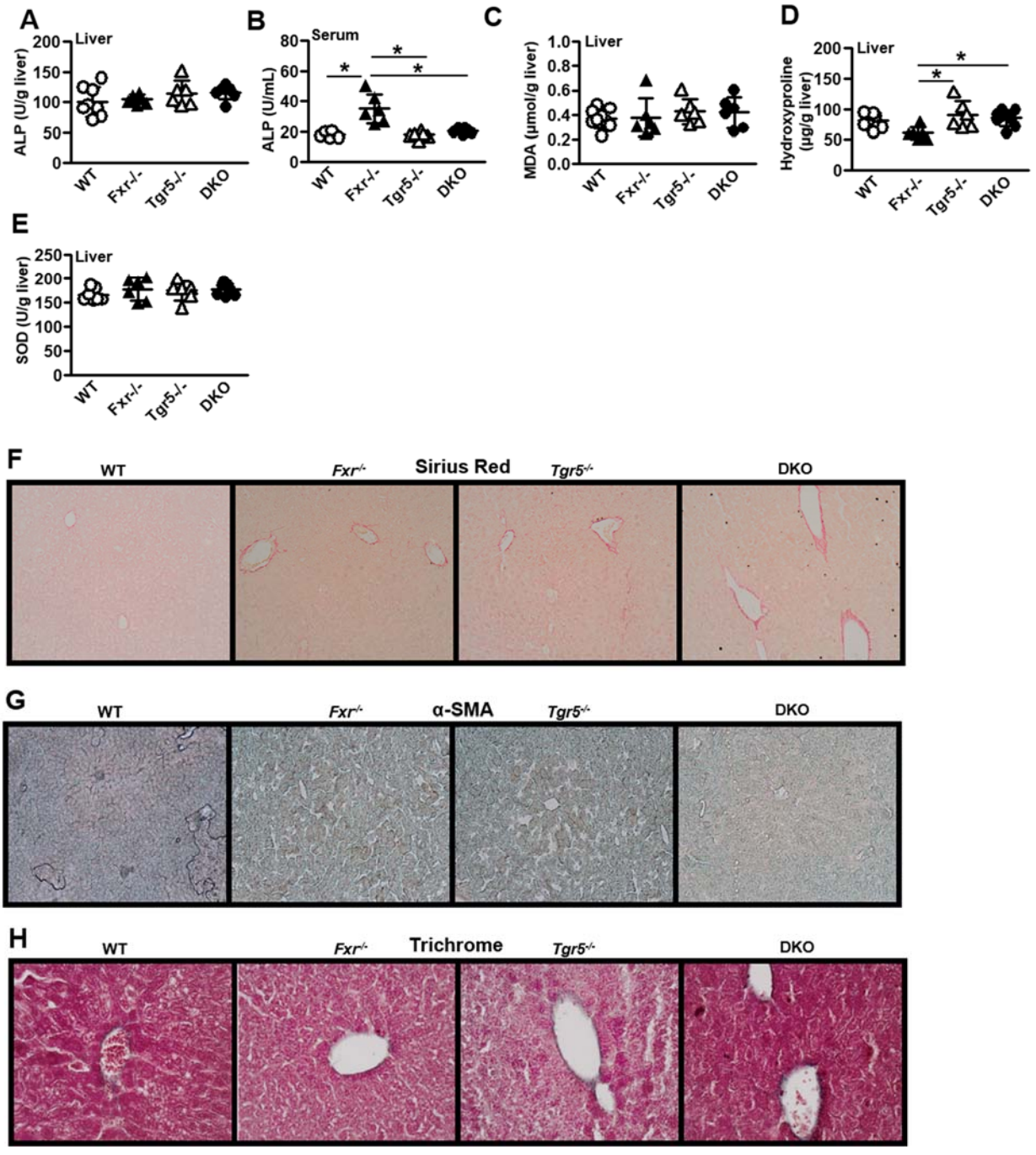

Supplemental Figure 3. Male wild type, *Fxr*$^{-/-}$, *Tgr5*$^{-/-}$, and *Fxr*$^{-/-}$/*Tgr5*$^{-/-}$ (DKO) mice, n=6-9. **A.** Alkaline phosphatase (ALP) in liver (left) and serum (right). **C.** Liver malondialdehyde indicative of thiobarbituric acid reactive substances (TBARS). **D.** Liver hydroxyproline. **E.** Liver superoxide dismutase activity. **F.** Representative image of liver Sirius Red staining (10x). **G.** Representative

image of liver α-SMA staining (10x). **H.** Representative image of liver Masson's trichrome staining (20x). WT, wild type mice; Fxr-/-, Fxr single knockout mice; Tgr5-/-, Tgr5 single knockout mice, DKO, *Fxr*$^{-/-}$/*Tgr5*$^{-/-}$ double knockout mice; ***** indicates $p<0.05$.

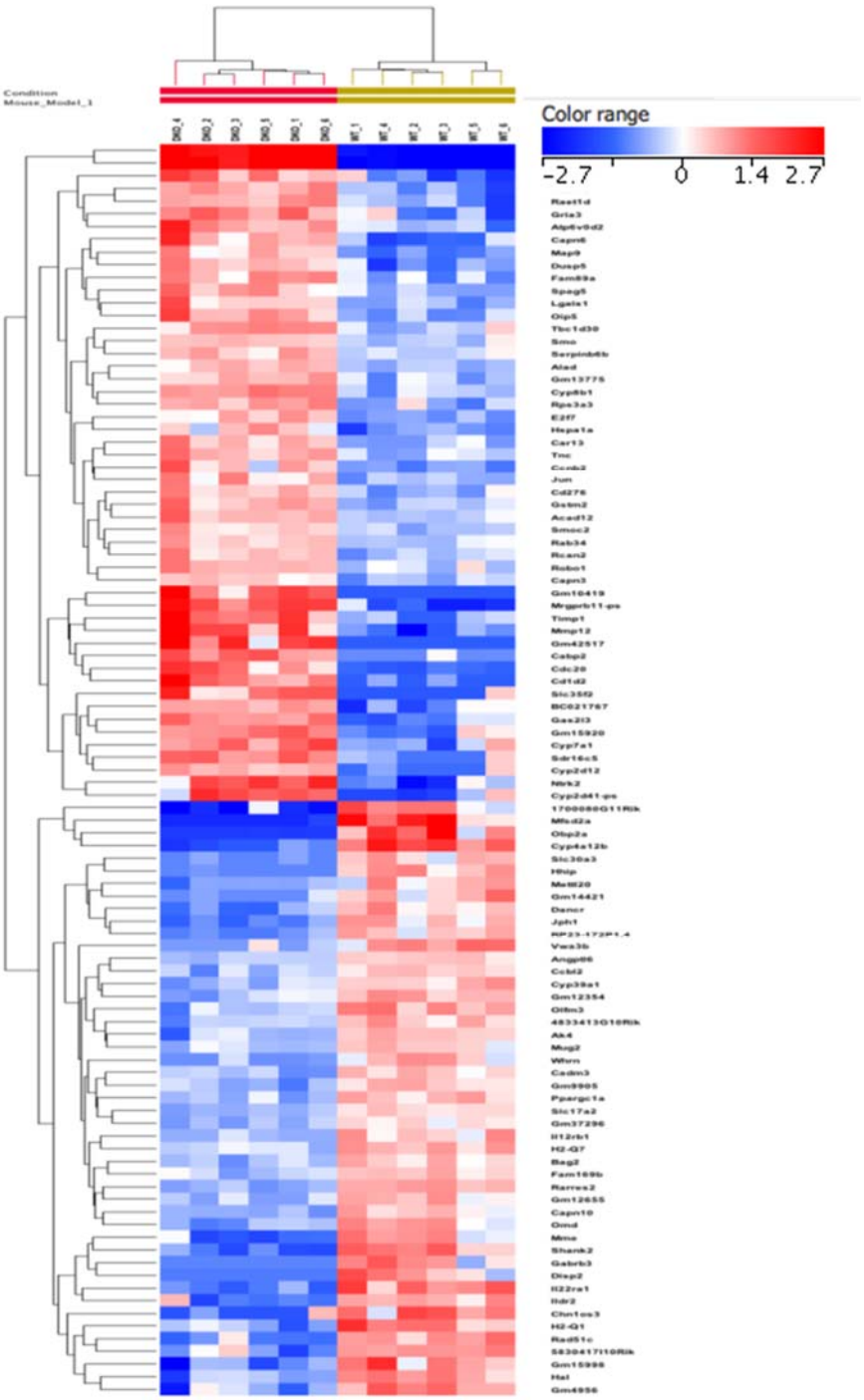

Supplemental Figure 4. Heatmap of unique differentially expressed genes (DEGs) in adult male wild type vs DKO mice. Moderated FDR-corrected *t*-test (cut-off=p<0.05) >2.0 fold change. Gene-level analysis from RNA-seq data using Cuffnorm, 99 DEGs.

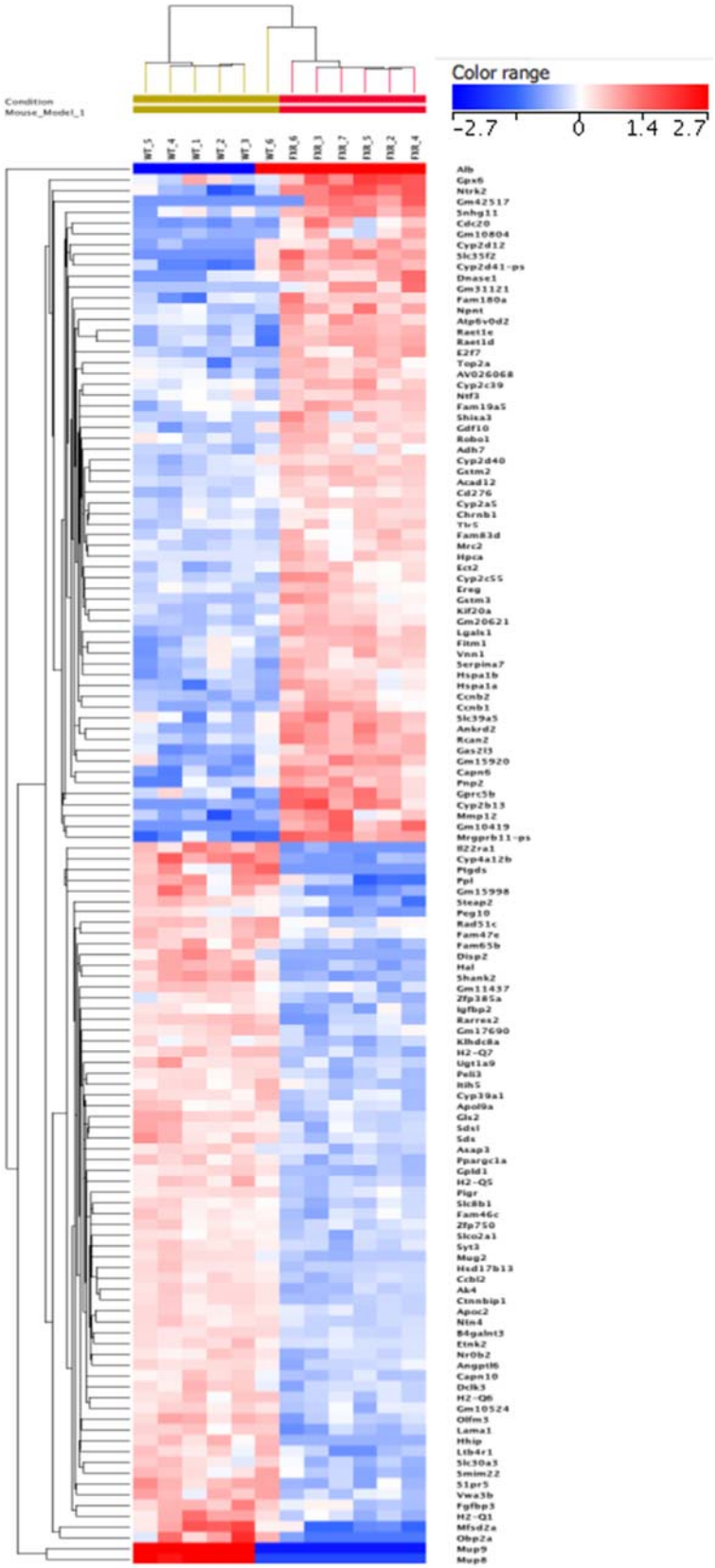

Supplemental Figure 5. Heatmap of DEGs, *Fxr*$^{-/-}$ vs. WT mouse liver. FDR corrected, *t*-test (p<0.05), >2.0-fold change. Gene-level analysis from RNA-Seq data using Cuffhorm, 130 DEGs.

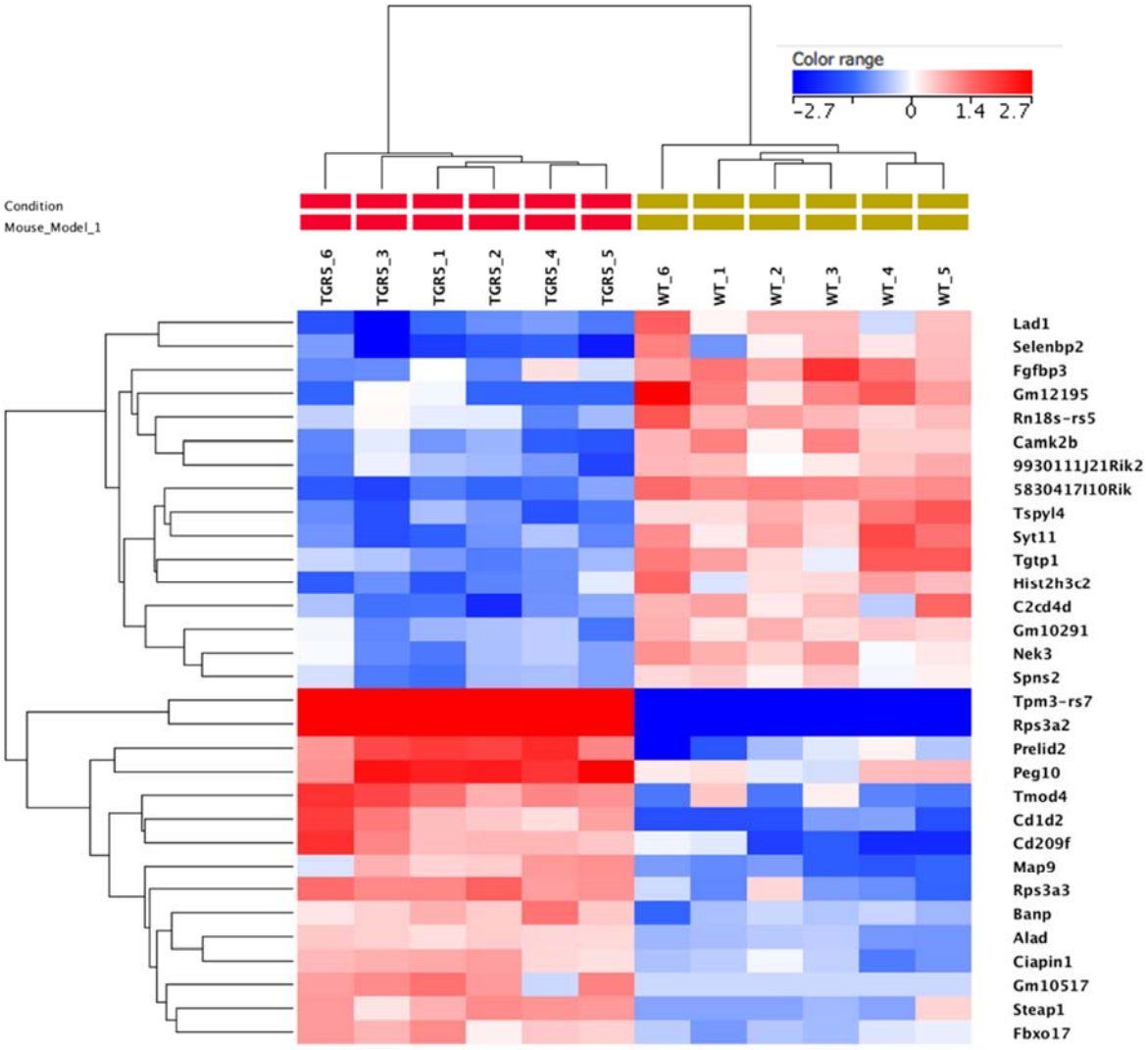

Supplemental Figure 6. Heatmap of DEGs, *Tgr5*$^{-/-}$ vs. WT mouse liver. FDR corrected, *t*-test (p<0.05), >2.0-fold change. Gene-level analysis from RNA-Seq data using Cuffnorm, 31 DEGs.

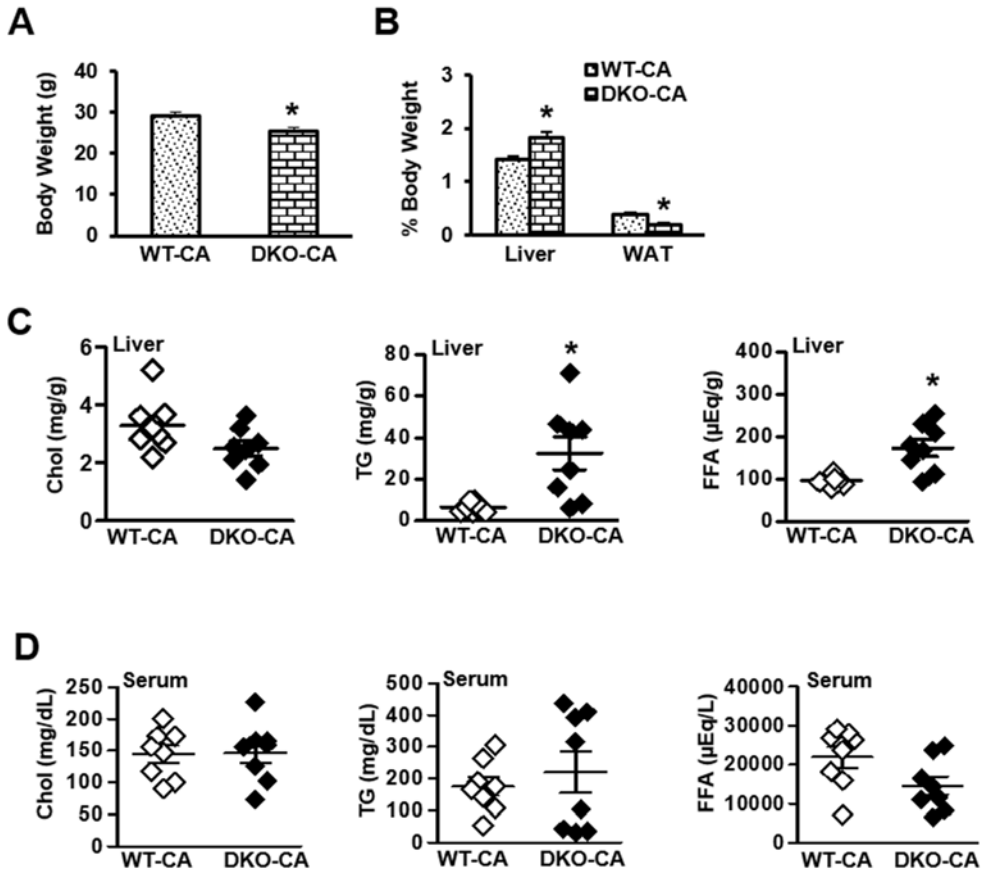

Supplemental Figure 7. Male wild type and *Fxr*$^{-/-}$/*Tgr5*$^{-/-}$ mice were fed cholic acid (0.5% for 2 weeks), n=9. **A.** Body weight. **B.** Liver and white adipose tissue (WAT) weight expressed as a percentage of body weight. **C.** Liver cholesterol (left), triglycerides (middle), and free fatty acids (right). **D.** Serum cholesterol (left), triglycerides (middle), and free fatty acids (right). WT-CA, wild type mice fed cholic acid; DKO-CA, *Fxr*$^{-/-}$/*Tgr5*$^{-/-}$ double knockout mice fed cholic acid; * indicates $p<0.05$.

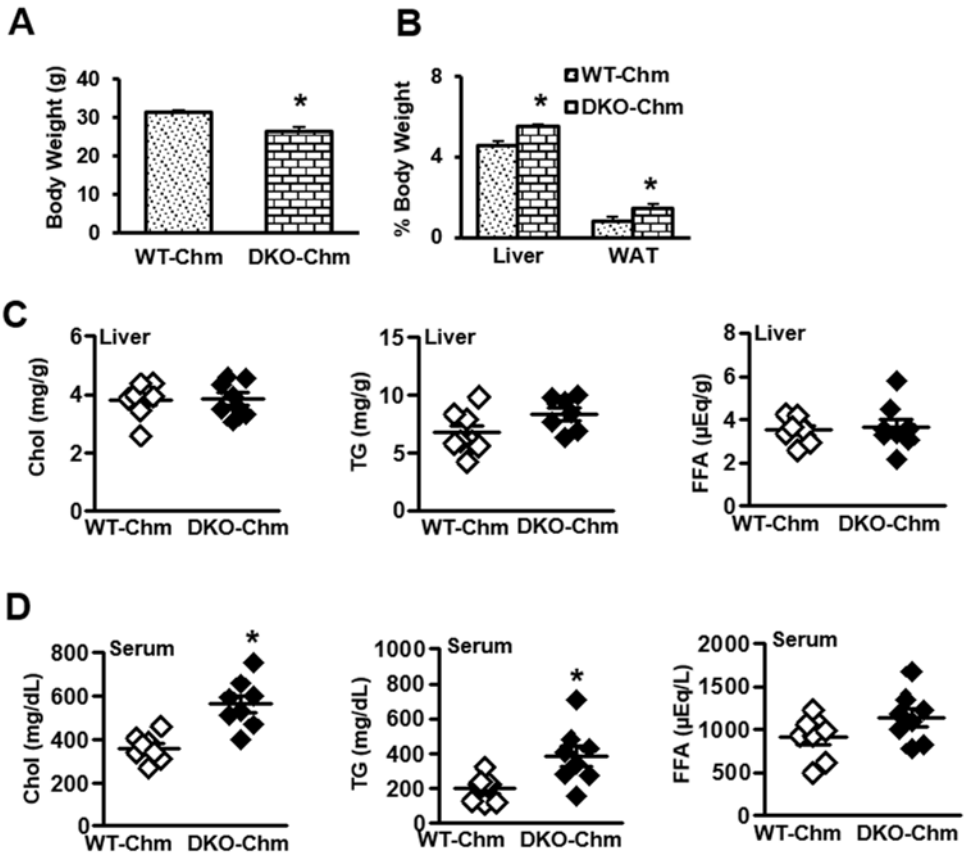

Supplemental Figure 8. Male wild type and *Fxr*$^{-/-}$/*Tgr5*$^{-/-}$ mice were fed the bile acid sequestrant cholestyramine for 2 weeks, n=8. **A.** Body weight. **B.** Liver and white adipose tissue (WAT) weight expressed as a percentage of body weight. **C.** Liver cholesterol (left), triglycerides (middle), and free fatty acids (right). **D.** Serum cholesterol (left), triglycerides (middle), and free fatty acids (right). WT-Chm, wild type mice fed cholestyramine; DKO-Chm, *Fxr*$^{-/-}$/*Tgr5*$^{-/-}$ double knockout mice fed cholestyramine; * indicates $p<0.05$.

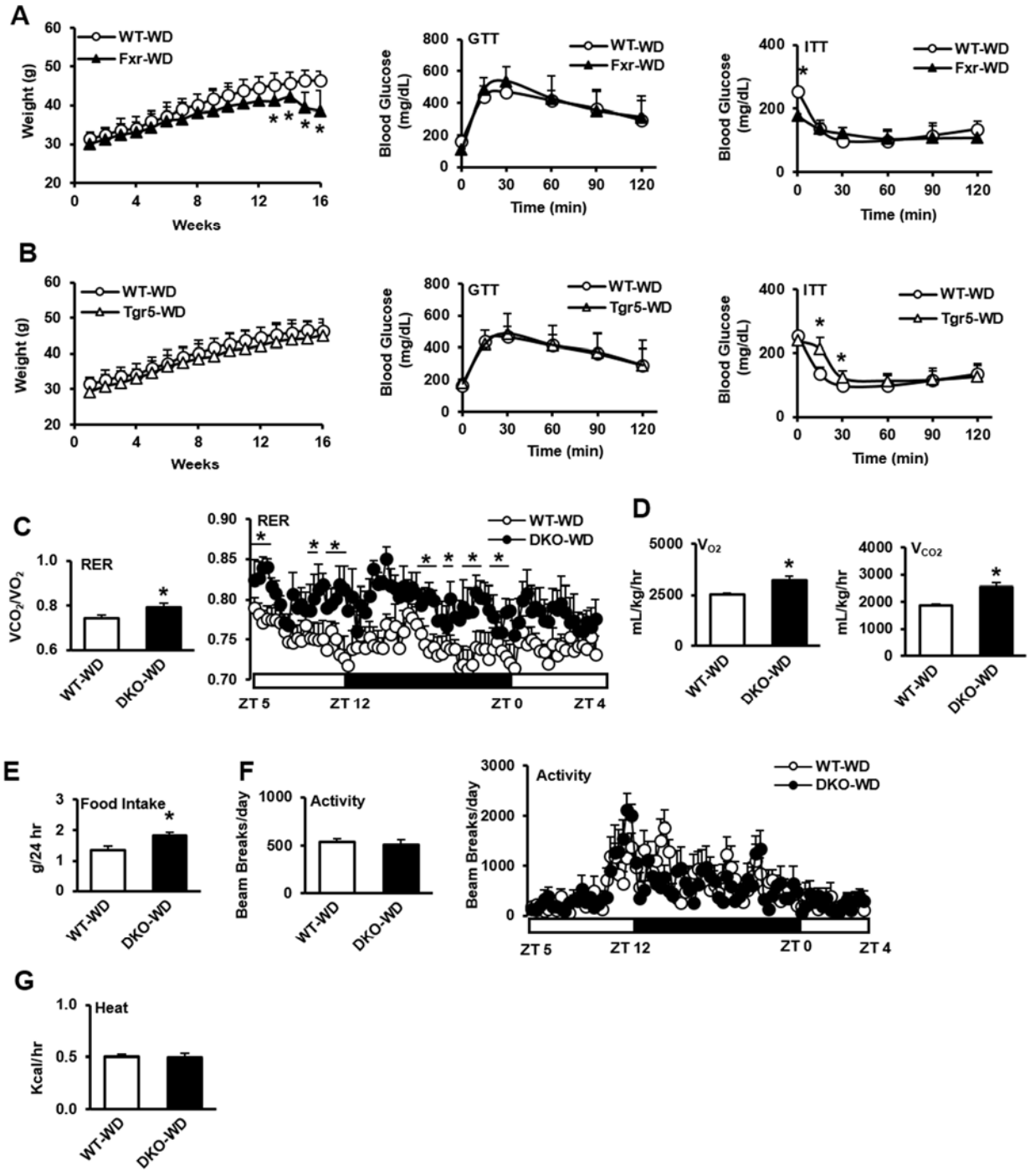

Supplemental Figure 9. Male wild type, *Fxr*$^{-/-}$, *Tgr5*$^{-/-}$, and *Fxr*$^{-/-}$/*Tgr5*$^{-/-}$ (DKO) mice were fed high-fat Western diet (42% kcal from fat, 0.2% cholesterol) for 16 weeks, n=5-8. **A.** Male wild type and *Fxr*$^{-/-}$ mouse body weight (left), glucose tolerance test (middle) and insulin tolerance test (right). **B.** Male wild type and *Tgr5*$^{-/-}$ mouse body weight (left), glucose tolerance test

(middle) and insulin tolerance test (right). **C.** Respiratory exchange ratio (left) and over 24 hr (right). **D.** Average oxygen consumption (left) and carbon dioxide production (right). **E.** Average food intake. **F.** Total average daily locomotor activity (left) and over 24 hr (right). **G.** Average heat production. WT-WD, wild type mice fed Western diet; Fxr-WD, *Fxr*$^{-/-}$ mice fed Western diet; Tgr5-WD, *Tgr5*$^{-/-}$ mice fed Western diet; DKO-WD, *Fxr*$^{-/-}$/*Tgr5*$^{-/-}$ double knockout mice fed Western diet; ***** indicates $p<0.05$.

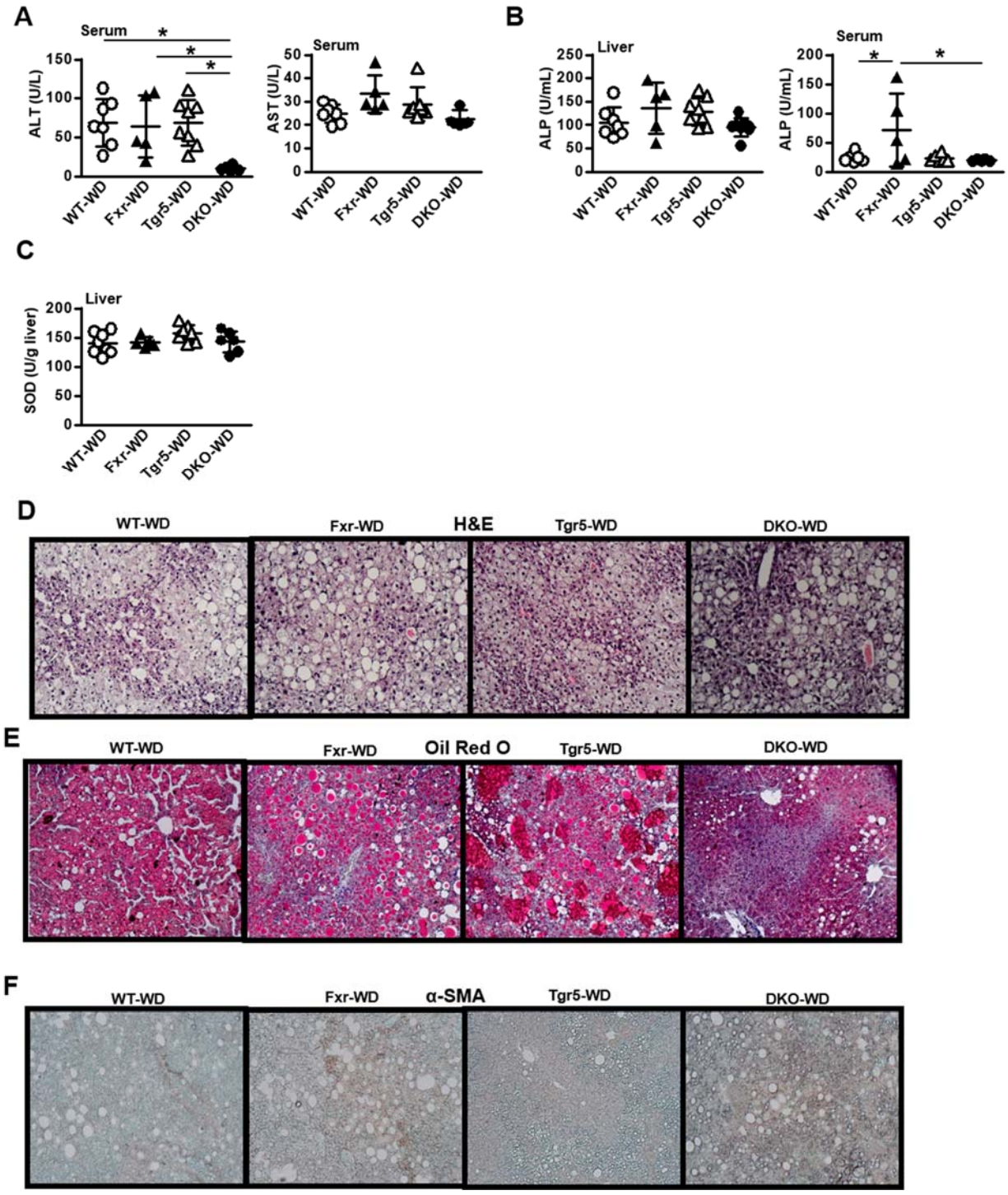

Supplemental Figure 10. Male wild type, *Fxr*$^{-/-}$, *Tgr5*$^{-/-}$, and *Fxr*$^{-/-}$/*Tgr5*$^{-/-}$ (DKO) mice were fed high-fat Western diet (42% kcal from fat, 0.2% cholesterol) for 16 weeks, n=5-8. **A.** Serum aspartate aminotransferase (AST, left) and alanine aminotransferase (ALT, right). **B.** Alkaline

phosphatase (ALP) in liver (left) and serum (right). **C.** Liver superoxide dismutase (SOD) activity. **D.** Representative image of liver hematoxylin & eosin staining (10x). **E.** Representative image of liver Oil Red O staining (10x). **F.** Representative image of liver α-smooth muscle actin (α-SMA, 10x) staining. WT-WD, wild type mice fed Western diet; Fxr-WD, *Fxr*$^{-/-}$ mice fed Western diet; Tgr5-WD, *Tgr5*$^{-/-}$ mice fed Western diet; DKO-WD, *Fxr*$^{-/-}$/*Tgr5*$^{-/-}$ double knockout mice fed Western diet; ***** indicates $p<0.05$.

Supplemental Table 1

Top-regulated pathways and diseases in *Fxr*$^{-/-}$ Mice

Pathway	Database	p-value
Cell cycle	BioSystems: KEGG	3.99E-08
Mitotic G1-G1/S phases	BioSystems: REACTOME	2.22E-07
G1/S transition	BioSystems: REACTOME	4.59E-07
DNA replication	BioSystems: REACTOME	1.76E-06
Cell cycle	BioSystems: REACTOME	2.12E-06
M/G1 transition	BioSystems: REACTOME	3.91E-06
DNA replication pre-initiation	BioSystems: REACTOME	3.91E-06
Regulation of DNA replication	BioSystems: REACTOME	3.94E-06
Assembly of the pre-replicative complex	BioSystems: REACTOME	4.54E-06
Cell cycle, mitotic	BioSystems: REACTOME	4.88E-06
Cell cycle checkpoints	BioSystems: REACTOME	4.97E-06
S phase	BioSystems: REACTOME	7.68E-06
CDC6 association with the ORC:origin complex	BioSystems: REACTOME	8.93E-06
Synthesis of DNA	BioSystems: REACTOME	9.00E-06
G2/M checkpoints	BioSystems: REACTOME	1.77E-05
Activation of BH3-only proteins	BioSystems: REACTOME	2.57E-05
Transcriptional regulation by TP53	BioSystems: REACTOME	2.78E-05
Orc1 removal from chromatin	BioSystems: REACTOME	3.54E-05
Switching of origins to a post-replicative state	BioSystems: REACTOME	3.54E-05
Removal of licensing factors from origins	BioSystems: REACTOME	4.82E-05
Apoptosis	BioSystems: REACTOME	6.26E-05
Mitotic G2-G2/M phases	BioSystems: REACTOME	6.46E-05
Programmed cell death	BioSystems: REACTOME	8.17E-05
Intrinsic pathway for apoptosis	BioSystems: REACTOME	9.27E-05
Activation of ATR in response to replication stress	BioSystems: REACTOME	1.19E-04
Activation of the pre-replicative complex	BioSystems: REACTOME	2.31E-04
Unwinding of DNA	BioSystems: REACTOME	2.62E-04
E2F mediated regulation of DNA replication	BioSystems: REACTOME	3.62E-04
G2/M transition	BioSystems: REACTOME	3.86E-04
CDT1 association with the CDC6:ORC:origin complex	BioSystems: REACTOME	4.32E-04

Supplemental Table 2

Top-regulated pathways and diseases in *Tgr5*$^{-/-}$ Mice

Pathway	Database	p-value
Oxidative phosphorylation	BioSystems: KEGG	1.74E-07
Non-alcoholic fatty liver disease (NAFLD)	BioSystems: KEGG	2.27E-07
Metabolic pathways	BioSystems: KEGG	1.56E-06
Parkinson's disease	BioSystems: KEGG	2.45E-06
Alzheimer's disease	BioSystems: KEGG	1.47E-05
Apoptosis	BioSystems: KEGG	3.56E-05
Neurotrophin signaling pathway	BioSystems: KEGG	6.56E-05
Huntington's disease	BioSystems: KEGG	1.59E-04
Antifolate resistance	BioSystems: KEGG	5.47E-04
Respiratory electron transport, ATP synthesis by chemiosmotic coupling, and heat production by UCPs	BioSystems: REACTOME	1.25E-08
The citric acid cycle and respiratory electron transport	BioSystems: REACTOME	6.89E-08
Gene expression	BioSystems: REACTOME	1.26E-07
Respiratory electron transport	BioSystems: REACTOME	1.58E-06
Chromatin organization	BioSystems: REACTOME	2.62E-05
Chromatin modifying enzymes	BioSystems: REACTOME	2.62E-05
Deubiquitination	BioSystems: REACTOME	4.36E-05
Macroautophagy	BioSystems: REACTOME	6.20E-05
Complex I biogenesis	BioSystems: REACTOME	1.28E-04
Transcriptional regulation by TP53	BioSystems: REACTOME	1.34E-04
Membrane trafficking	BioSystems: REACTOME	1.62E-04
Metabolism of proteins	BioSystems: REACTOME	2.21E-04
Fatty acid, triacylglycerol, and ketone body metabolism	BioSystems: REACTOME	2.78E-04
Metabolism of amino acids and derivatives	BioSystems: REACTOME	2.99E-04
Formation of ATP by chemiosmotic coupling	BioSystems: REACTOME	3.11E-04
Processing of capped intron-containing pre-mRNA	BioSystems: REACTOME	3.86E-04
Defects in biotin (Btn) metabolism	BioSystems: REACTOME	5.50E-04
Defective HLCS causes multiple carboxylase deficiency	BioSystems: REACTOME	5.50E-04
Vesicle-mediated transport	BioSystems: REACTOME	5.51E-04
Leigh disease	DisGeNET Curated	8.07E-09
Muscle hypotonia	DisGeNET Curated	1.48E-08
Cognitive delay	DisGeNET Curated	1.94E-06
Mental and motor retardation	DisGeNET Curated	1.94E-06
Low intelligence	DisGeNET Curated	2.47E-06
Dull intelligence	DisGeNET Curated	2.47E-06
Poor school performance	DisGeNET Curated	2.47E-06
Mental deficiency	DisGeNET Curated	2.78E-06
Intellectual disability	DisGeNET Curated	3.40E-06
Low posterior hairline	DisGeNET Curated	3.47E-06
Mitochondrial respiratory chain defects	DisGeNET Curated	3.64E-06
Mental retardation	DisGeNET Curated	8.23E-06
Global developmental delay	DisGeNET Curated	9.14E-06
Epilepsy	DisGeNET Curated	1.37E-05
Cardiomyopathies	DisGeNET Curated	1.67E-05
Pachygyria	DisGeNET Curated	2.55E-05
Dystonia	DisGeNET Curated	3.64E-05
Scotoma, centrocecal	DisGeNET Curated	5.54E-05
Seizures	DisGeNET Curated	8.30E-05
Optic Atrophy	DisGeNET Curated	9.72E-05
Retinal telangiectasia	DisGeNET Curated	1.04E-04
Acidosis, lactic	DisGeNET Curated	1.20E-04

References

1. Pathak P, Cen X, Nichols RG, Ferrell JM, Boehme S, Krausz KW, et al. Intestine farnesoid X receptor agonist and the gut microbiota activate G-protein bile acid receptor-1 signaling to improve metabolism. Hepatology. 2018, in press.
2. Levin JZ, Yassour M, Adiconis X, Nusbaum C, Thompson DA, Friedman N, et al. Comprehensive comparative analysis of strand-specific RNA sequencing methods. Nat Methods. 2010;7(9):709-15.
3. Borodina T, Adjaye J, Sultan M. A strand-specific library preparation protocol for RNA sequencing. Methods Enzymol. 2011;500:79-98.
4. Pertea M, Kim D, Pertea GM, Leek JT, Salzberg SL. Transcript-level expression analysis of RNA-seq experiments with HISAT, StringTie and Ballgown. Nat Protoc. 2016;11(9):1650-67.
5. Kim D, Langmead B, Salzberg SL. HISAT: a fast spliced aligner with low memory requirements. Nat Methods. 2015;12(4):357-60.
6. Pertea M, Pertea GM, Antonescu CM, Chang TC, Mendell JT, Salzberg SL. StringTie enables improved reconstruction of a transcriptome from RNA-seq reads. Nat Biotechnol. 2015;33(3):290-5.
7. Frazee AC, Pertea G, Jaffe AE, Langmead B, Salzberg SL, Leek JT. Ballgown bridges the gap between transcriptome assembly and expression analysis. Nat Biotechnol. 2015;33(3):243-6.
8. Chen J, Bardes EE, Aronow BJ, Jegga AG. ToppGene Suite for gene list enrichment analysis and candidate gene prioritization. Nucleic Acids Res. 2009;37(Web Server issue):W305-11.
9. Subramanian A, Tamayo P, Mootha VK, Mukherjee S, Ebert BL, Gillette MA, et al. Gene set enrichment analysis: a knowledge-based approach for interpreting genome-wide expression profiles. Proc Natl Acad Sci U S A. 2005;102(43):15545-50.
10. Ashburner M, Ball CA, Blake JA, Botstein D, Butler H, Cherry JM, et al. Gene ontology: tool for the unification of biology. The Gene Ontology Consortium. Nat Genet. 2000;25(1):25-9.
11. Chiang JY. Reversed-phase high-performance liquid chromatography assay of cholesterol 7α-hydroxylase. Methods in enzymology. 1991;206:483-91.